Nationaal Lucht- en Ruimtevaartlaboratorium
National Aerospace Laboratory NLR

NLR-TP-2002-273

Miniature loop heat pipe with a flat evaporator

Thermal modelling; Experimental results

A.A.M. Delil and V. Baturkin

Nationaal Lucht- en Ruimtevaartlaboratorium
National Aerospace Laboratory NLR

NLR-TP-2002-273

Miniature loop heat pipe with a flat evaporator

Thermal modelling; Experimental results

A.A.M. Delil and V. Baturkin*

* National Technical University of Ukraine "Kyiv Polytechnic Institute KPI"

This report contains two papers. The first one was presented at the 32th International Conference on Environmental Systems (San Antonio, Texas, 14-18 July 2002). The second one was presented, as invited lecture, during the 12th International Heat Pipe Conference (Moscow - Kostrama - Moscow, 19-24 May 2002). The reported activities pertain to the final reporting of the INTAS-UKRAINE project 95-0196.

Customer:	National Aerospace Laboratory NLR
Working Plan number:	R.1.A.1
Owner:	National Aerospace Laboratory NLR
Division:	Space
Distribution:	Unlimited
Classification title:	Unclassified
	Julye 2002

Summary

This report contains two papers, being:
- "Modelling of a Miniature Loop Heat Pipe with a Flat Evaporator", presented at the 32th International Conference on Environmental Systems (San Antonio, Texas, 14-18 July 2002).
- "Experiments on Heat transfer Phenomena in a Miniature Loop Heat Pipe with a Flat Evaporator", presented at the 12th International Heat Pipe Conference (Moscow, Kostrama, Moscow, 19-24 May 2002).

The reported activities were carried out within the INTAS-UKRAINE project 95-0196 "Research of Heat & Mass Transfer Processes in Passive Two-Phase Systems for Heat Transportation and Temperature Control for Usage in Energy Saving Equipment", by a team led by the project co-ordinator and scientific responsible, A.A.M. Delil (NLR). The Ukrainian team, leader was V. Baturkin (National Technical University of Ukraine "Kyiv Polytechnic Institute KPI"). Other Ukrainian contributors to the project were employed at KPI (O. Habatuk, Yu. Friedrichson, Yu. Khmelev, V. Kravec, D. Oliferenko, V. Savina, A. Savchenko, K. Shcoda, S. Zhuk and T. Zinchenko), at the National Space University "Kharkiv Aviation Institute" (G.A. Gorbenko, P.G. Gakal, K.A. Malukhin, V.I. Ruzaykin, N.I. Ivanenko, E.I. Ganja, N.A. Nrus, A.P. Sazonov and K.S. Epifanov), and at the "Institute for Low-Temperature Physics and Engineering of the National Academy of Sciences of Ukraine (V.V. Abraimov and L. Kolibaev).

Contents

(19 pages in total)

SAE-2002-01-2506

Modelling of a Miniature Loop Heat Pipe with a Flat Evaporator

A.A.M. Delil
National Aerospace Laboratory NLR, Netherlands

V. Baturkin
National Technical University of Ukraine "Kyiv Polytechnic Institute", Kyiv, Ukraine

G. Gorbenko, P. Gakal, V. Ruzaykin
National Aerospace University "Kharkiv Aviation Institute", Kharkiv, Ukraine

ABSTRACT

The classic design of a loop heat pipe usually includes a cylindrical evaporator design, where the heat generated at the wall has thermal/hydraulic contact with the surface of a cylindrical porous wick structure. Such a design is characterised by good technological and physical bases and well-proven theory. It is capable to solve many tasks in various applications.

But also attempts to design a loop heat pipe with flat interfaces between the heated wall and wick are of practical interest for applications, for which the effective heat input to a cylindrical evaporator surface is hardly or not realisable, or for which the mounting surfaces require a contact over a flat surface. World wide there is only limited development of flat-evaporator loop heat pipes: Hence this study can be called a novelty. Besides of technological development the basis for physical modelling of such loop heat pipe should be elaborated. One possible approach, based on the method of idealised elements for pressure and temperature prediction, is presented.

INTRODUCTION

The majority of loop heat pipe (LHP) designs utilises a cylindrical evaporator, in which the "heat generating" wall has good contact to the cylinder surface of the porous wick body. Such a design has a good technological and physical basis and is supported by a well-proven theory, allowing to apply such a configuration to execute many practical tasks. Anyhow, attempts to design a loop heat pipe with a flat "heating wall-wick" contact surface are very scarce [1], but certainly of practical interest for applications where the effective heat inputs to cylindrical evaporator surface are hardly or not realisable, or where the mounting surfaces require the contact over flat surface only. Also the study of adapting the main known design principles and techniques to a flat heat transfer arrangement is a very interesting subject of research.

The reported research approach on a LHP with a flat evaporator was divided into several stages. During the first stage the following tests with different types of capillary structures were performed: Investigation of the pore size distribution, the maximum diameter bubble test, and the measurement of the liquid permeability in the direction of filtration. Potential porous candidate structures have been fabricated of nickel, titanium powder, from stainless fibres and Teflon, in a flat cylindrical shape, with a diameter around 40 mm and a thickness from 4 to 7 mm. The maximum pore diameters of the investigated structures cover a range from 2 to 60 microns. After this the most attractive candidates have been studied in a special test bed to define the heat transfer efficiency, for a flat contact between heating surface and a porous structure. Experiments have been performed with ethanol at a constant pressure of 0.3 Bar, for heat fluxes up to 30 W/cm^2. The different variants of configurations of the porous structure and the substrate have been studied to define the optimum between the technological fabrication complexity and thermal efficiency. Based on the obtained results, the experimental model of a LHP has been prepared. The flat evaporator design, size ∅ 44 x 22 mm, allows easy replacement of the porous structure. The test range includes heat fluxes up to 30 W/cm^2 in any orientation with respect to gravity. The modelling liquid was ethanol. The experimental results confirm the possibility to realise a heat transfer flat contact of 10 to 30 kW/m^2.K, at fluxes of 10 to 15 W/cm^2. The experimental model of the loop heat pipe was able to start with a power of less than 10 W. It shows stable operation for of 50 to 70 W, and 1 m against gravity. The obtained results suggest that it will be possible to design very powerful loop heat pipes with a flat thermal contact to the heat source.

The experimental activities were supported by the development of a LHP mathematical model, based on the "idealised-elements" method. The description of this approach, to simulate either the temperature or the pressure distribution over the LHP elements and the generalised characteristics, is presented in detail.

EXPERIMENTAL APPROACH

Experimental activities concentrated on the study of structural characteristics of porous materials for the capillary pump, and on a heat exchange study for conditions, typical for a flat contact to the capillary medium substrate. Apart from the self-standing interest for such information, the results of this activity were used for the definition of the unknown heat transfer coefficients in the LHP theoretical model.

STRUCTURAL AND HYDRODYNAMIC CHARACTERISTICS OF POROUS SAMPLES

A list of the majority of the tested samples is presented in table 1. The sintered felt materials and most of powder have been manufactured and studied at the National Technical University of Ukraine "Kyiv Polytechnic Institute".

Table 1. List of various porous materials tested

Structure Type	Material	ε, %	D_{max}, μm	$K*10^{14}$ m^2
Felt	Ni	81	116	3550
Felt	X18H9T	66	66	2340
Felt	X20H80	66	90	3360
Felt	Ni	50	62	773
Felt	Ni	35	14	0.31
Felt	SS	45	3.8	6.7
Powder	Ni	34	2	0.28
Powder	Ni	54	4	4.4
Powder	Ni	42	3.3	3.6
Powder	Ni	51	4.8	8.5
Powder	Ni	47	2	2
Powder	Ni	48	4.3	3.3
Powder	Ni	46	4.3	2.2
Powder	Ni	43	6.6	15.2
Powder	X20H80	36	12	24.5
Powder	Ni	66	2.4	2.0
Powder	Ti	57	10.4	20

The methods and test beds for measuring hydrodynamic properties were elaborated according recommendations given in E128 of the ASTM Committee. The main results can be summarised by:

- Metal felt capillary structures with fibre diameters of 20-50 microns, within the investigated range of porosity (50- 80%), have a maximal pore size D_{max} between 60 and 116 microns, which is equivalent to an elevation height for ammonia of 0.12 to 0.24 m (at 20 ^{0}C). This value is small enough for LHP operation against gravity forces. Therefore this type of capillary structure is to be preferred for horizontal/near-horizontal LHP orientation.
- High values of wick permeability (up to $35*10^{-12}$ m^2) allow the use of a small (available) pressure head for the liquid to move in the pipelines.
- Porous structures made from powders have a maximal pore size D_{max} ranging from 2 to 12 microns, which is equivalent to an elevation height for ammonia from 1.5 to 8 m (+ 20 ^{0}C). They are suitable for operation of LHP against gravity. The permeability of samples lays in the range from 0.25 .to. $24 \cdot 10^{-14}$ m^2.
- Further development of metal felt samples design and technology allows to reduce the pore maximal sizes to 3 – 8 microns and to reach the permeability typical for powder samples at the same maximum pore diameters. These samples are suitable for operation of a LHP against gravity.

HEAT TRANSFER STUDY

The characterisation and optimisation of heat transfer at the flat interface between the heated surface and the porous structure plays an important role in LHP design. The experimental modelling of a flat thermal contact and the evaporation processes for inverted meniscus conditions has been performed in the test bed shown in figure 1.

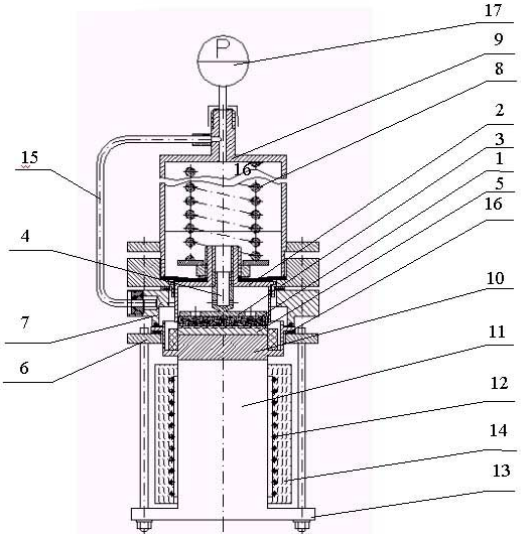

Figure 1. Working section of test bench for research on heat exchange by evaporation: 1 - Capillary structure (CS) sample; 2 - Yoke; 3 - Punched plate; 4 - Hollow screw; 5 - Finned substrate; 6, 7 - Flanges; 8 - Spring; 9 - Condenser; 10 - Block for heat flux measurement; 11 - Heater; 12 – Ni-chrome winding; 13 - Flange; 14 - Layer of thermal insulation; 15 - Vapour line; 16 - Rubber pad; 17 - Vacuum gauge

The CS sample 1 (typical diameter 39 mm) was placed in a special yoke 2, so that the end face of the sample was projected from the yoke on 1 - 2 mm. Positioning of the samples of various thickness inside the yoke 2 was done by transition of the punched plate 3, with the help of screw 4. For a liquid flow from the condenser to the porous sample the screw 4 was hollow with holes at the bottom. The sticking out of the yoke end face of the CPS sample was pressed to the finned side of substrate 5 by bolts through the flanges 6 and 7. There the pressing force was by a spring 8, placed inside the condenser 9.

The smooth side of a substrate was soldered to the block of heat flux measurement 10. The heater 11 represents the copper cylinder with the Ni-chrome winding 12 and

flange 13. The outside of the heater was covered with a layer of thermal insulation 14. The thermal contact of the heater 11 with the block 10 was provided by pressing through a heat-conducting paste by means of the flanges 6 and 13. The grooves between edges of a substrate were for removal of vapour (generated in CPS sample), saturated with the heat-carrier. The evaporation zone and condensation zone were interconnected by the vapour line 15. The vapour line had transparent sections to visualise the process. The tightness of assembly was achieved by using vacuum rubber pads 16 at the junctions of all elements of the working section. Most parts (except the heater, vapour line and copper casing of the condenser) were fabricated of stainless steel. To decrease the heat losses to the environment, the working section was heat-insulated outside by basalt mattresses. The system pressure was controlled by the vacuum gauge 17.

The schematic of the thermocouple layout on the working section is shown in figure 2. The heated substrate has a smooth side and a profiled side, interfacing with capillary structure. On the smooth substrate side, two copper-constantan thermocouples 1 were caulked, whose average indications allowed to define the temperature of the heated surface. In the top of the heat flux measurement block parallel to its end faces a hole was drilled, and in the lower end face the groove was made.

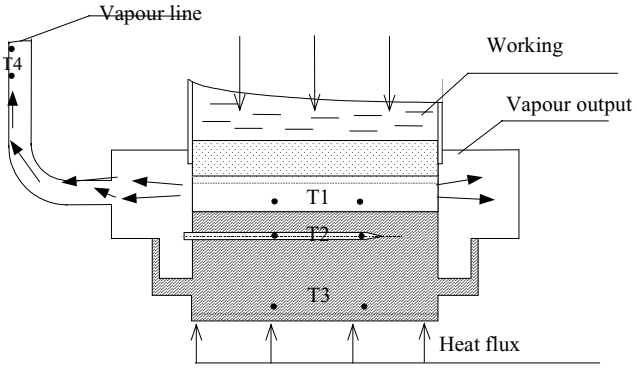

Figure 2. Schematic of thermocouple layout on the test bench working section, for studying heat exchange during vaporisation

In a hole and groove another copper-constantan thermocouples (respectively 2 and 3) were installed for definition of transmitted heat power. The vapour temperature was read by the thermocouple 4, located on the vapour line.

Several conclusions were obtained during this research:
- Metal felt samples provided the higher heat transfer intensity during boiling in comparison to powder samples, under similar conditions.
- For the metal felt samples, the heat transfer coefficients reached values of 7 to 10 kW/m^2.K at the maximum heat flux density q = 120 kW/m^2
- For the powder samples the heat transfer coefficients were far less than the corresponding values for the metal felt samples at the maximum heat flux densities q = 30 to 60 kW/m^2
- Improvement of the contact of the CS with a substrate (by sintering) for felt samples resulted in an increase of the heat transfer coefficients, in comparison with pressing the samples to substrate. For the powder samples, sintering lead to some decrease of the heat transfer intensity
- Combined structures “powder substrate plus felt on the outer layer” allowed to considerably intensify the heat transfer process, as compared to the powder samples.

The detailed analysis of the obtained experimental data on heat exchange, e.g. the description of function of heat transfer on heat flux density, maximal reached heat flux density, and influence of conditions of contact “porous structure-substrate” are out of the scope of the aim of this paper. It will be discussed in future publications.

LHP NUMERICAL MODELLING

The mathematical model of the LHP was being developed according to the method of idealised elements [2,3]. Within this concept, all physical elements of the LHP are replaced by one, or by several idealised elements. All idealised elements can be divided in two groups:

- Elements modelling the thermal hydraulic processes in working fluid.
- Elements modelling the heat transfer processes between design elements or between design elements and the working fluid.

The first group of idealised elements forms a hydraulic network, and the other one forms a thermal network. The hydraulic network and the thermal network constitute the nodal model, a graphical image of a mathematical model, and is individual for each heat transfer device. The form of the nodal model and the number of idealised elements depend on information, which should be obtained as a result of the mathematical modelling. The basic idealised elements of the hydraulic network are control volumes and branches (Fig. 3). The control volume is an open thermodynamic system with a fixed volume, which is defined by a set of state parameters (pressure, internal energy), and described by two equations: continuity and energy. The branch transfers mass and energy between control volumes. It has only one inlet and one outlet, and is described by the momentum equation.

The thermal network consists of thermal nodes and heat conductors. Thermal nodes are defined only by the temperature and described by the heat balance equation.

The coupling of hydraulic network and thermal network is by “heat conductors”, idealised elements which model a heat transfer between the design wall and working fluid.

The equations describing the steady-state processes in idealised elements can be written as (Fig. 5):

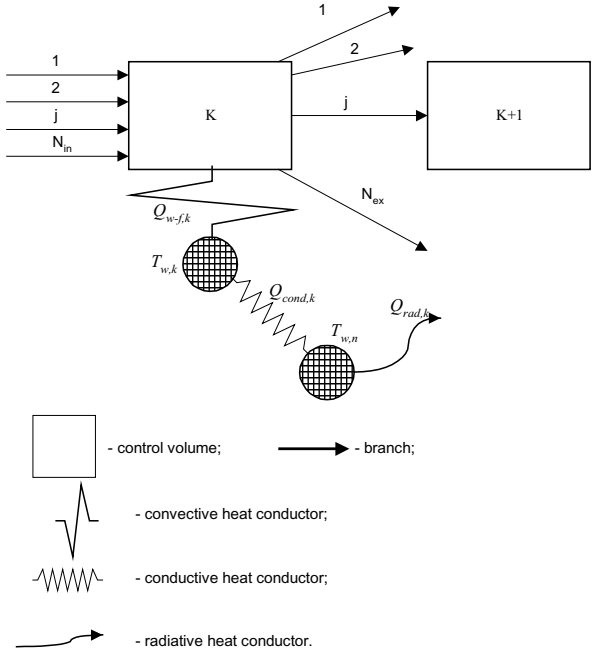

Figure 3. Idealised elements of the nodal model

1) The continuity equation of an arbitrary volume *k,* fixed in a space is:

$$\sum_{j=1}^{N_{in}} m_j - \sum_{j=1}^{N_{ex}} m_j = 0\,, \qquad (1)$$

where $\sum_{j=1}^{N_{in}} m_j$ is the algebraic sum of the working fluid mass rates (kg/s), which enter the control volume *k,* through the branches adjoined to it.

$\sum_{j=1}^{N_{ex}} m_j$ is the algebraic sum of working fluid mass rates (kg/s), which exit *k* through the branches connected to it.

2) The energy equation for control volume *k*:

$$\sum_{j=1}^{N_{in}} m_j \cdot i_j^* - \sum_{j=1}^{N_{ex}} m_j \cdot i_k^* \pm Q_{w-f,k} + L = 0\,, \qquad (2)$$

where $\sum_{j=1}^{N_{in}} m_j \cdot i_j^*$ is the algebraic sum of energies, internal, kinetic, and surface energy (W), which come into *k* through the branches connected to it.

$\sum_{j=1}^{N_{ex}} m_j \cdot i_k^*$ is the algebraic sum (internal, kinetic and surface energy (W), which exit *k* through the branches connected to it.

$Q_{w-f,k}$ is the heat flux (W) from wall to working fluid, *L* is the rate of mechanical work (W).

It is assumed that i_j^* is the stagnation enthalpy (J/kg)of the working fluid in the control volume, from which the *j* branch exits.

3) The branch is described by the momentum equation and characterised only by mass flow rate m_j. The momentum equation for the branch is:

$$P_k - P_{k+1} + \Delta P_a + \Delta P_f + \Delta P_g + \Delta P_p = 0\,. \qquad (3)$$

4) The thermal node is described by the energy equation for the stationary heat conducting medium. The energy equation for heat node *k* is:

$$\sum_{i=1}^{N_{in}} Q_i - \sum_{i=1}^{N_{ex}} Q_i = 0\,, \qquad (4)$$

where $\sum_{i=1}^{N_{in}} Q_i$ is the algebraic sum of heat fluxes (W), which enter the node through the heat conductor connected to it.

$\sum_{i=1}^{N_{ex}} Q_i$ is the algebraic sum of heat fluxes (W), which exit the heat node via the heat conductors connected to it.

The coupling of control volume with heat node, and also coupling between heat nodes are realised by means of “heat conductor idealised elements”. According to the type of heat transfer, heat conductors are divided in the following groups:

- Heat conductors, in which heat transfer is realised by convection:

$$Q_{w\text{-}f,k} = \alpha_k \cdot F_{w,k} \cdot (T_{w,k} - T_{f,k})\,, \qquad (5)$$

where α_k is the heat transfer coefficient in heat conductor the *k* (W/m^2·K).
$F_{w,k}$ is the heat transfer area (m^2) of heat conductor *k.*
$T_{w,k}$ is the temperature (K) of thermal node *k.*
$T_{f,k}$ is the temperature of working fluid (K) in control volume *k.*

- Heat conductors, in which heat transfer is by conduction:

$$Q_{cond,k} = \lambda \cdot \frac{F_{cond,k}}{l_{cond,k}} \cdot \left(T_{w,k} - T_{w,n}\right) \text{ for a flat surface} \qquad (6)$$

$$Q_{condk} = \frac{\lambda \cdot F_{condk}}{r_k ln(1+\frac{l_{condk}}{r_k})} \cdot \left(T_{w,k} - T_{w,n}\right) \text{ for a cylinder surface (7)}$$

where $F_{cond,k}$ is the heat transfer area (m^2) of heat conductor k, $T_{w,n}$ is the temperature (K) of thermal node n, λ is the thermal conductivity (W/m·K), $l_{cond,k}$ is the distance (m) between nodes k and n, $r_{,k}$ is the radius (m) of the thermal node k.

- Heat conductors, in which heat transfer is realised by thermal radiation to the surroundings:

$$Q_{rad,k} = \varepsilon_k \cdot \sigma \cdot F_{rad,k} \cdot \left(T_{w,k}^4 - T_{sur}^4\right) \quad (8)$$

where $F_{rad,k}$ is the heat transfer area (m^2) of the heat conductor k, T_{sur} is the temperature (K) of the surroundings (SUR), ε_k is the surface emissivity, and σ=5.67·10^{-8} W/(m^2·K^4) is the Stefan-Boltzmann constant.

The mathematical model includes the system of the equations (1) to (8), complemented with the equations of state, relations for the calculation of thermophysical properties, the friction coefficient in pipes and capillary structures, and relations for the calculation of heat transfer coefficients.

Let us use the suggested mathematical model to analyse the distribution of parameters and to obtain the steady-state characteristics of the LHP with a flat evaporator. The principal LHP schematic is shown in figure 4. All elements are horizontally, but the analysis can also be applied to different allocations of the evaporator and condenser. For the calculation example considered, the material of the wick is stainless steel powder (X18H80). Parameters of the wick are: Porosity 36%, permeability K = 2.45·10^{-13} m^2, average pore diameter D_{av}=12.0 μm, effective thermal conductivity λ=3.5 W/m·K.

The nodal scheme (graphical image of the mathematical model), which allows to solve the aforementioned problems, is shown in figure 7. The idealised elements, modelling the heat transfer in the evaporator, are shown in figure 7, for a geometry similar to the corresponding real elements. Thus the 1st thermal node corresponds to the heat supply flange, the 10th node corresponds to the heat transfer surface. Nodes 2 - 8 pertain to the evaporator body, node 9 is the cover, 11 and 12 pertain to the vapour line wall within evaporator, and 13 - 15 pertain to the capillary structure (wick).

In the working fluid circulation loop: The vapour line is represented by the control volumes 6 to 8 and the branches 6 to 8, the liquid line by the control volumes 1,17,18 and the branches 1, 17 and 18. The condenser consists of the control volumes 9 to 16, the branches 9 to 16 and. and the heat conductors 39 to 46. The capillary structure consists of the control volumes 3, 4, 19 and 5, plus the branches 3, 4, 19 and 5. The compensation chamber and the area before the capillary structure are represented by the control volumes 2 and 20, and the branches 2 and 20. The heat transfer is modelled by the heat conductors 1 to 46. To take into account the environmental influence, the control volume *EV* has been added into the nodal model schematic. Heat transfer coefficients of the heat conductors are calculated by the corresponding relations for the type of heat transfer (conduction, convection). The heat transfer coefficients values, calculated on the data [4], are given in table 2.

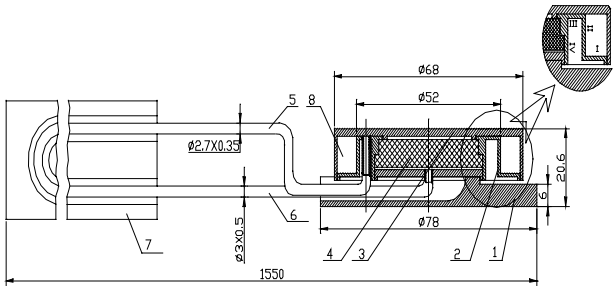

Figure 4. LHP Schematic 1 - Heat supply flange; 2-Body; 3 – Cover; 4 – Capillary structure (CS); 5 – Liquid line; 6 – Vapour line; 7 – Condenser; 8 – Compensation Chamber (CC).

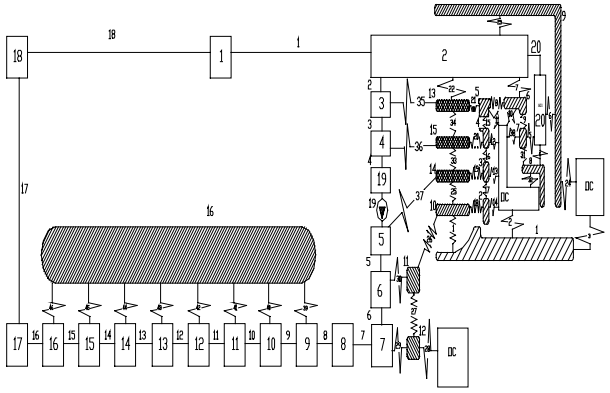

Figure 5. Nodal model of LHP

Heat transfer coefficient of condensation in a horizontal condenser can be written as [5]:

$$\alpha_{cond} = M^2 \left(T_{sat} - T_w\right) L^{0.35} D^{-0.5}, \text{ W/m}^2\text{·K}, \quad (9)$$

where T_{sat} is the saturation temperature (K), T_w is the wall temperature (K), L is the condenser length (m) and D is the diameter of the condenser (m).

M is the coefficient, which depends on the working fluid thermophysical properties and condensation temperature

$$M = 1.4654 \cdot \frac{\lambda_L \rho_L^{0.1}}{\left(l \cdot \nu_L\right)^{0.5} \rho_v^{0.3} \sigma^{0.3}}, \quad (10)$$

where, ρ_L and ρ_v are the liquid density and vapor density, respectively;
ν_L is the kinematic viscosity(m^2/s). λ_L is the thermal conductivity (W/m·K), σ is the surface tension (N/m) and l is the latent heat (J/kg).

Pressure losses in the branches are calculated according to equations for flow in horizontal pipes.

Table 2. Characteristics of the heat conductors

№	Modelling details on thermal conductance	W/K
1.	Heat transfer between the heat input flange and the heat transfer surface	12.76
2.	Heat transfer from flange to SUR (from side surface and surface faced to evaporator body)	0.21
3.	Heat transfer between the flange side surface and SUR	0.027
4.	Heat transfer between 1st section of evaporator body and working fluid in CC	0.705
5.	Heat transfer between 2nd section of the evaporator body and working fluid in CC	0.852
6.	Heat transfer between the evaporator cover and working fluid in CC	0.141
7.	Heat transfer between 3rd section of evaporator body and working fluid at entrance of wick	0.132
8.	Heat transfer between sections 3 and 4 of the evaporator body	2.74
9.	Heat transfer between sections 2 and 3 of the evaporator body	2.5
10.	Heat transfer between section 3 of the evaporator body and SUR	0.0186
11–14.	Heat transfer between section 4 of the evaporator body and SUR	0.0077
15 –17.	Heat transfer of heat nodes in section 4 of the evaporator body	1.91
18.	Heat transfer between the heat transfer surface and 4th section of the evaporator body	18.25
19–21.	Heat transfer between the wick and 4th section of the evaporator body	0.069
22.	Heat transfer between wick and working fluid at the wick entrance	0.098
23.	Heat transfer coefficient between working fluid at the entrance of the wick and the cover	0.24
24.	Heat transfer coefficient between cover and SUR	0.4
25.	Heat transfer between heat transfer surface and the wick	0.88
26.	Heat transfer between heat transfer surface and vapour line	15.28
27.	Heat transfer in the vapour line within the evaporator	0.009
28.	Heat transfer between vapour line and SUR	0.0038
29.	Heat transfer between vapour line wall and vapour	0.036
30.	Heat transfer between vapour line wall and vapour	0.0045
31.	Heat transfer between the sections 1 and 2 of the evaporator body	1.2
32.	Heat transfer between section 1 of the evaporator body and SUR	0.029
33–34.	Heat transfer in the wick	0.38
35–37.	Heat transfer between the wick and the working fluid in the wick	65000
38.	Heat transfer between section 2 of the evaporator body and SUR	0.0346
39 - 46.	Heat transfer between the condenser body and the working fluid	see [4, 5]

To model the pressure losses in the two-phase flow, the two-phase multiplier Φ_{LO}^2 t is introduced, assuming that the two-phase flow is homogeneous:

$$\Phi_{LO}^2 = \left[1 + x\left(\frac{\rho_L}{\rho_v} - 1\right)\right] \cdot \left[1 + x\left(\frac{\mu_L}{\mu_v} - 1\right)\right]^{-0.25} \qquad (11)$$

where μ_L,μ_v are the liquid and vapour dynamic viscosity respectively (N·s/m^2), x is the vapour quality;

Pressure losses in the flat capillary structure are [6]:

$$\Delta p_f = m \cdot \frac{\mu_L}{C_{fL}\rho_L} \qquad (12)$$

$$C_{fL} = \varepsilon \cdot A \cdot \frac{K}{L} \qquad (13)$$

where, m is the mass flow rate (kg/s) and A is the wick total frontal area (m$^{2)}$.

The system consists of 72 equations for control volumes, branches, heat nodes and equations, which follow from the conditions of vapour quality before the meniscus $x_{19}=0$, and after the meniscus $x_5=1$. The final system of equations consists of 74 non-linear algebraic equations. The system of non-linear equations was solved by a standard numerical method (the modified Powell hybrid algorithm) in the library of standard procedures of the Fortran Power Station programming language. Mass flow rates in branches, pressures and enthalpies in control volumes, temperatures in heat nodes and heat fluxes in heat conductors were calculated.

The pressure distributions in the working fluid and the working fluid temperature along the LHP are shown in figures 6 a,b, for the heat loads Q_Σ= 5 W and Q_Σ= 150 W. The results show that the largest pressure losses are in the wick (Δp = 210 Pa for Q_Σ = 5 W and Δp = 7600 Pa for Q_Σ = 150 W) and in the vapour line (Δp =10 Pa for Q_Σ= 5 W and Δp = 100 Pa for Q_Σ= 150 W). Pressure losses in the liquid line are considerably less then those in the wick and the vapour line. This is due to the small mass flow rates: m = $1.66 \cdot 10^{-6}$ kg/s for a heat load of 5 W, $7.85 \cdot 10^{-5}$ kg/s for 150 W). The main temperature change occurs in the wick. In the vapour line the working fluid temperature increases by heat fluxes from the heat transfer surface. In the condenser, the condensation heat transfer coefficient is considerably larger than the one for super-cooling. This is why the main heat removal is in the condensation section. The condensation length is approx. 0.4 m for a heat load of 5 W, 0.6 m for 150 W. The temperature change in the super-cooling section is negligible due to very small heat removal.

To estimate LHP efficiency the stationary characteristic is used: $R = f(Q_\Sigma)$, where Q_Σ is the heat load (W) and $R = (T_{w,1} - T_{w,16})/Q_\Sigma$ is LHP thermal resistance (K/W). The steady-state characteristic is shown in figure 7. The dependence of heat fluxes in the CC, heat losses to the environment and the heat removal by the condenser of the heat load of the LHP are shown in figure 8.

The P-T state diagram of processes in the LHP at heat load 150 W is shown in figure 9. Point 1 on the saturation curve is related to the vapour parameters over the meniscus. The section 1-2 is related to pressure losses in vapour removal channels. The section 2-3 is related to the vapour motion through the vapour line, where pressure drops due to losses and temperature increasing due to heat fluxes from the heat transfer surface occur. The section 3-4-5 is related to heat removal in condenser (3-4 is the heat removal in condensation part and 4-5 is in the super-cooling part). Point 5 coincides with point 6 due to small pressure losses and heat removal in the liquid line. Point 7 is related to the wick inlet. Due to heat flux from the wick the working fluid increases. Pressure at the point 7 is the same as at the point 6. The section 7-8 of diagram is related to heating of working fluid temperature to the saturation state and to pressure drops in the wick. The pressure drop in the section 8-1 corresponds to the capillary pressure.

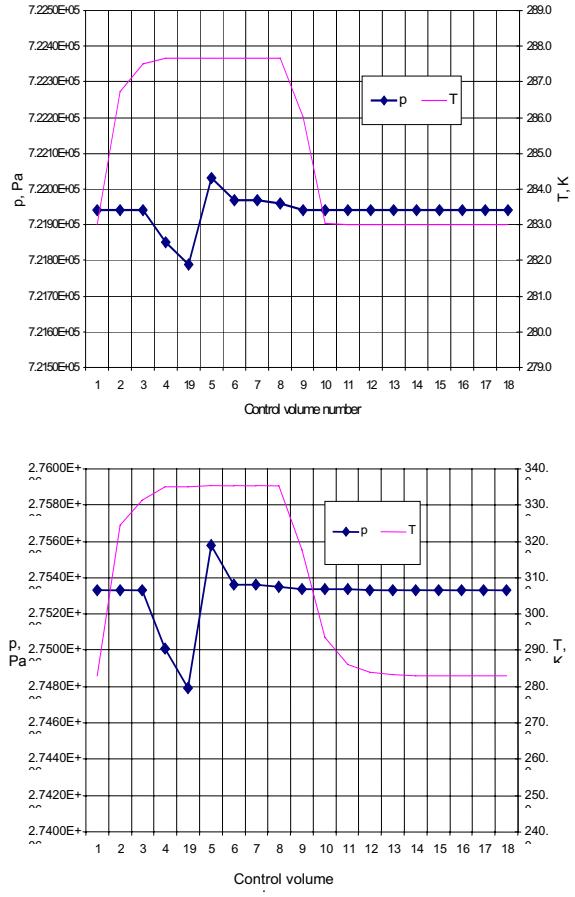

Figure 6. Pressure/temperature distribution along LHP for: $Q_{\square}$=5 W (upper figure) and $Q_{\square}$=150 W b (bottom)

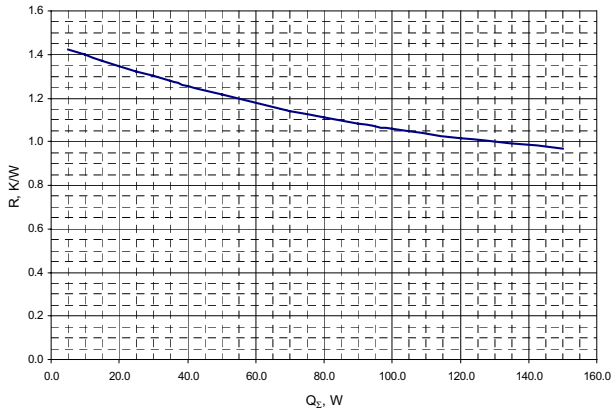

Figure 7. Steady-state thermal resistance of LHP

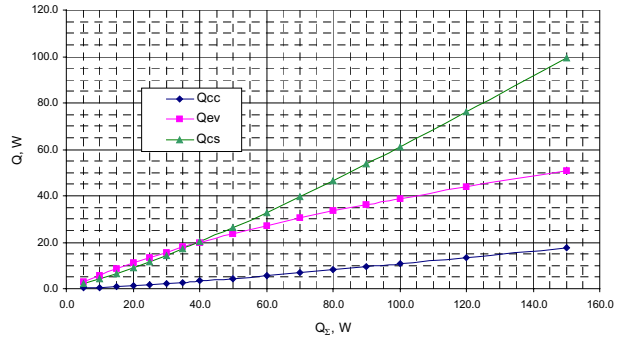

Figure 8. LHP power dependence of heat fluxes in CC, heat losses to environment and condenser heat removal

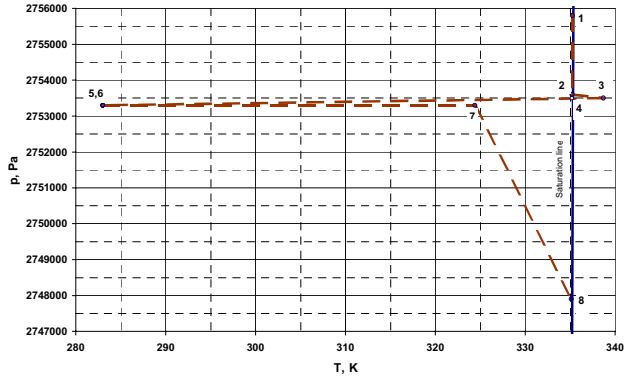

Figure 9. The P-T state diagram of processes in LHP, at 150 W heat load

The approach for numerical LHP simulation could be useful for its comprehensive analysis, for the prediction of distributed parameters (temperature, pressure) and for the prediction of generalised characteristics: Overall thermal resistance and maximal power transferred.

CONCLUSION

The review of experimental activities to design the LHP with a flat interface between capillary structure and heated surface is presented in brief only. The approach to simulate the thermal behaviour by nodal modelling (system discretisation) has been demonstrated. The

output of the model are the steady state distributed and generalised parameters, which are the result of a LHP experimental mock-up simulation.

ACKNOWLEDGEMENT

The research has been done in a joint project (INTAS-Ukraine 95-196) of the International Association for the promotion of co-operation with scientists from the New Independent States of the former Soviet Union (INTAS) and the Ukrainian Ministry of Education and Science,

REFERENCES

1. Yu. Maidanik, S. Vershinin, M. Chernisheva. Development and tests of Miniature Loop heat Pipe with a Flat evaporator. Proceedings of the 30 th Int. Conf. on Environmental Systems and 7th European Symp. on Space Environmental Systems. July 10-13, 2000, Toulouse, France, Paper N 2001-01-2491.
2. P.Gakal, G.Gorbenko. Mathematics and physical modeling of complicated heat energy system / In digest “Udoskonalennja turboustanovok metodamy matematychnogo modelyuvannya” – Kharkiv: Instute for mashinebuilding problems named A.M.Pidgorny, National Academy of Science of Ukraine, 2000, pp. 69–75.
3. V. Blinkov. Modelling of nonsteady thermodynamic processes in heat exchange contours with two phase flow. // Atomic Energy. - Moscow, 1992. Volume 73. Issue 6, pp. 439-442.
4. V.Isachenko, V.Osipova, A.Sukomel. Heat transfer.– Moscow, Mir Publishers, 1969, - 552 p.
5. Refrigeration. Encyclopedic vocabulary «Technika proizvodsva iskustvennogo holoda», Vol. 1. Moscow, Gostorgizdat, 1960. – 544 pages.
6. B. Gullimore. SINDA-FLUINT. User’s manual.

CONTACT

Dr. V.Baturkin, National Technical University of Ukraine “Kyiv Polytechnic Institute”, Peremogy Pr., 37, 03056, Kyiv, Ukraine. Email: baturkin@carrier.kiev.ua

Experimental Results on Heat Transfer Phenomena in a Miniature Loop Heat Pipe with a Flat Evaporator

A.A.M. Delil
National Aerospace Laboratory NLR, Space Division
P.O.Box 153, 8300 AD Emmeloord, Netherlands
Phone: +31 527 248229; Fax: +31 527 248210; E-mail: adelil@nlr.nl

V. Baturkin, Yu. Friedrichson, Yu. Khmelev, S. Zhuk
National Technical University of Ukraine "Kyiv Polytechnic Institute"
Peremogy Pr.37, Kyiv -56, 03056, Kyiv, Ukraine
Phone/Fax: 380-44 2417597; E-mail: baturkin@carrier.kiev.ua

Abstract

The basic design of a loop heat pipe usually concerns a cylindrical evaporator design, in which the "heat generating" wall has a good contact to the cylinder surface of the porous wick body. Such a design has a good technological and a physical basis and is supported by a well-proven theory, yielding solutions for many practical applications. However, attempts to design a loop heat pipe with a flat "heating wall-wick" interface are of practical interest for those applications, for which the effective heat inputs to cylindrical evaporator surface is hardly or not realisable, or for which the mounting surfaces request the contact over flat surface only. Also the study of adapting the main known design principles and techniques to a flat heat transfer arrangement is a very interesting subject of research. This research approach on a loop heat pipe with a flat evaporator was divided in several stages. The first stage of the investigations with different types of capillary structures consisted of the pore size distribution determination, the maximum pore diameter bubble test, and the measurement of the liquid permeability in the direction of filtration. Potential candidate porous structures, fabricated of nickel, titanium powder, stainless fibres and Teflon, in a flat cylindrical shape, were tested. The second stage consisted of experimenting with the most attractive candidate materials in a special test bed, in order to define the heat transfer efficiency for a flat interface between heating surface and porous structure. Experiments have been done with ethanol at a constant pressure of 0.3 Bar, for heat fluxes up to 30 W/cm^2. The third stage dealt with the integration of a flat porous structure in a loop heat pipe system and the study of heat transfer characteristics (the influence of heat flux and orientation). The experimental results confirm the objective: To realise a heat transfer of 10 to 30 kW/m^2 through the flat contact "substrate-porous structure", at fluxes of 10 to 15 W/cm^2. The experimental loop heat pipe model (diameter 44 mm, thickness 22 mm) turned out to be able to start at a power below 10 W. It showed stable operation against gravity (1 m elevation) for a power of 50 to 70 W.

INTRODUCTION

The basic design of a loop heat pipe (LHP) usually concerns a cylindrical evaporator, in which the "heat generated" wall has a good contact to the cylinder surface of the porous wick body. Such a design has a good technological and a physical basis and is supported by a well-proven theory, yielding solutions for many practical applications. But also attempts to design a LHP with a flat "heating wall-wick" interface are of interest for many practical applications, if the effective heat input to cylindrical evaporator surface is hardly or not realisable, or if the mounting surfaces request contact over flat surface only. Also the study of adapting known design principles and techniques to a flat heat transfer arrangement is a very interesting research issue. In spite of the wide implementation of a flat "heating surface - porous body" interface in capillary pump loops, this interface is very scarce in LHP technology.

Among available literature sources one can find many examples of flat heat pipe design and modelling [1, 2]. The scarceness of flat interface arrangements may be explained by the dominating traditional technology of cylindrical wick fabrication, the advantages of a symmetric substrate/wick (reciprocal) positioning, being typical for a cylindrical configuration, symmetry of liquid input in the evaporator, etc. So, the flat contact of a heated substrate and wick can meet additional technical difficulties for a practical realisation. Nevertheless, for some terrestrial and space applications it would be preferable to use

such LHP designs. Also the heat transfer issues in inverted meniscus conditions (which take place in the flat contact area) have an additional value for its use in heat exchange technology. The above has initiated our attempts to develop LHP samples to study their characteristics.

The research approach, for developing a LHP with a flat evaporator, was divided in three stages. During the first stage the following tests with different types of capillary structures (CS) were performed: Investigation of the porosity ε, the pore size distribution, definition of the maximum pore diameter d_{max} by a "bubble test", and the measurement of the liquid permeability K in the direction of filtration. Potential porous candidate structures have been fabricated from nickel, titanium powder, stainless steel fibres and Teflon, in a flat cylindrical shape with a diameter D around 40 mm and a thickness δ between 3,3 and 7 mm. The maximal pore size d_{max} varies from 2 to 120 microns.

During the second stage the aspects of heat transfer at a flat contact under inverted meniscus conditions were been studied. Experiments were done with promising types of porous samples, using ethanol as the test fluid (at a constant pressure of 0.3 Bar, for heat fluxes q up to 30 W/cm^2). The different configuration variants of porous structure and substrate were studied to define an optimum between the technological fabrication complexity and thermal efficiency.

The third stage concerned the development of methods to incorporate a porous structure in the hydraulic and thermal schematics of a LHP. The tests were conducted with four types of capillary structures, with ethanol as the working fluid. The changeable parameters were the heat flux, and the orientation relative to gravity. Thermal resistance and maximal transferred power were determined from experimental data.

STRUCTURAL CHARACTERISTICS OF POROUS SAMPLES

Most tested samples are listed in table 1. The sintered fibre and most powder samples were manufactured at Kiev Polytechnic Institute. The figures 1 and 2 show the surface appearance of powder and fibrous samples with nearly the same value of maximal pore diameter.

The methods and test beds for the measurement of hydrodynamic properties were developed very close to the recommendations E 128 of the ASTM Committee.

Table 1. List of various porous materials tested

Structure Type	Material	ε, %	d_{max}, μm	$K\ 10^{14}$ m^2
Fibers	Ni	81	116	3550
Fibers	X18H9T	66	66	2340
Fibers	X20H80	66	90	3360
Fibers	Ni	50	62	773
Fibers	Ni	35	14	0.31
Fibers	SS	45	3.8	6.7
Powder	Ni	34	2	0.28
Powder	Ni	54	4	4.4
Powder	Ni	42	3.3	3.6
Powder	Ni	51	4.8	8.5
Powder	Ni	47	2	2
Powder	Ni	48	4.3	3.3
Powder	Ni	46	4.3	2.2
Powder	Ni	43	6.6	15.2
Powder	X20H80	36	12	24.5
Powder	Ni	66	2.4	2.0
Powder	Ti	57	10.4	20

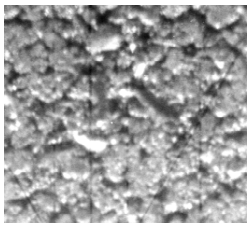

Figure 1. A powder sample of stainless steel: ε = 36 %, D = 38.8 mm, δ = 3,7 mm, d_{max} = 12.0 μm, K = $24.5 \cdot 10^{-14}$ m^2

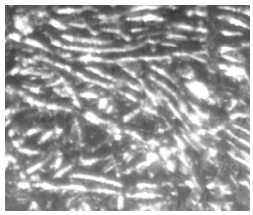

Figure 2. Metal fibre sample of nickel: ε = 35 %, D = 27.7 mm; δ = 13 mm; d_{max} = 13.5 μm, $K = 0.3 \cdot 10^{-14}$ m^2

The results obtained can be summarised by:

- Metal fibre capillary structures with fibre diameters between 20 and 50 microns (within the investigated range of porosity 50 to 80 %) have a maximum pore size d_{max} ranging from 60 to 116 microns, corresponding to an elevation height for ammonia of 0.12 to 0.24 m (at 20 ^{0}C). This value is small enough for LHP operation against gravity forces. Consequently this type of capillary structure is adequate for horizontal and near-horizontal LHP operation. High values of the wick permeability (till 35*10 $^{-12}$ m^2) allow the use of a small available pressure head for moving the liquid in the pipe lines;
- Porous structures of powder have maximum pore size d_{max} between 2 and 12 microns, corresponding to an elevation height for ammonia between 1.5 and 8.8 m (at 20 ^{0}C). This makes them suitable for LHP operation

against gravity. The permeability of the samples is in the range $(0.25 \text{ to } 24)\cdot 10^{-14}$ m^2.
- Further development of metal fibre sample technology will reduce maximum pore sizes till 3 to 8 microns, at permeability typical for powder samples for these diameters.

STUDY OF HEAT EXCHANGE AT A FLAT INTERFACE

The characterisation and optimisation of heat transfer at the flat contact of a heated surface and a porous structure plays an important role in LHP design. The experimental modelling of flat thermal interfaces and evaporation processes under inverted meniscus conditions has been performed in the following test bed (Fig. 3).

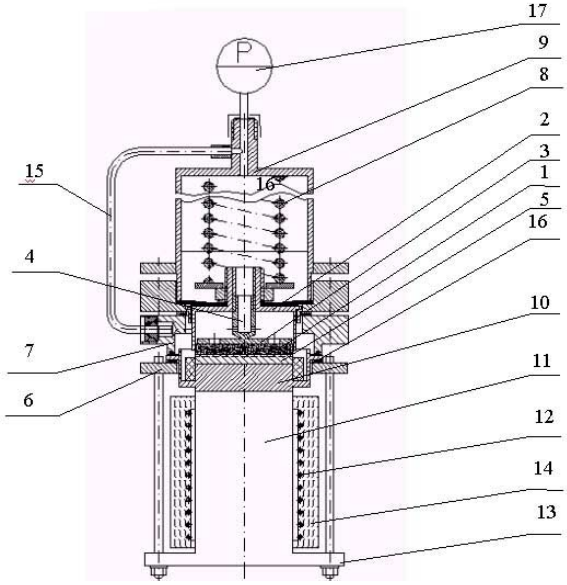

Figure 3. Working section of test bench for evaporation heat transfer research : 1 - CS sample; 2 - Yoke; 3 - Punched plate; 4 - Hollow screw; 5 - Finned substrate; 6, 7, 13 - Flanges; 8 - Spring; 9 - Condenser; 10 - Block for heat flux measurement; 11 - Heater; 12 – Ni-chrome winding; 14- Thermal insulation; 15 -Vapour line; 16 - Rubber pad; 17 - Vacuum gauge

The CS sample 1 (diameter ∅39 mm) is placed in a yoke 2, such that the sample end face sticks 1 to 2 mm out of the yoke. The positioning of samples (of different thickness) in the yoke 2 is adjusted by transition of punched plate 3 with screw 4. To allow liquid flow from condenser to porous sample, screw 4 is hollow with holes at the bottom. The from the yoke end face sticking out of the CS sample is pressed to the finned substrate side 5 by bolts through flanges 6 & 7. Pressing is provided by spring 8, placed inside the condenser 9.

The smooth side of the substrate is soldered to the heat flux measurement block 10. The heater 11 is the copper cylinder with Ni-chrome winding 12 and flange 13. The outside of the heater is covered with a layer of thermal insulation 14. The thermal contact of the heater 11 with the block 10 is provided by pressing (via heat-conducting copper powder paste) by means of flanges 6 and 13. The grooves between the edges of a substrate are for removal of vapour, generated in CPS sample, saturated with the heat-carrier. Evaporation and condensation zones are interconnected by the vapour line 15. For visualisation of a process, part of vapour line is transparent. Assembly tightness is achieved by using vacuum rubber pads 16, at the junctions of all working section elements. All details of this design (except the heater, vapour line and copper casing of the condenser) are stainless steel. To decrease heat losses to the environment outside the working section is thermally insulated by basalt cotton wool. The pressure in a system is controlled by pressure gauge 17.

The thermocouple locations in the working section are shown in figure 4. The draft of a substrate with channels for vapour removal is presented in figure 5. Two copper-constantan thermocouples 1 were caulked on the smooth side of the substrate basis. Their average defines the temperature of the heated surface. In the top of heat flux measurement block, parallel to its end faces, a hole was drilled. In the lower end face the groove was made. In hole and groove two copper-constantan thermocouples 2 and 3 were installed to measure the transported thermal power. The vapour temperature was measured by thermocouple 4, on the vapour line.

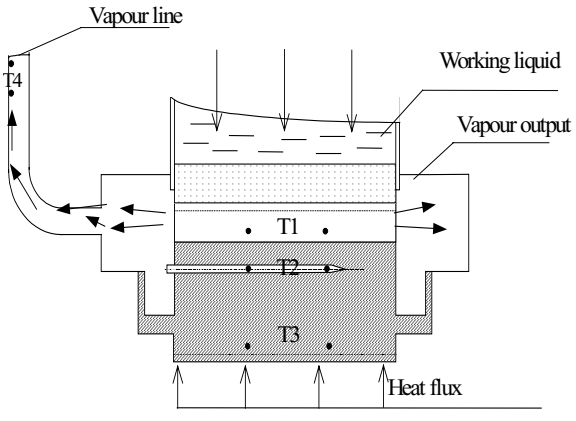

Figure 4. Thermocouple locations in the working section, to study evaporative heat transfer

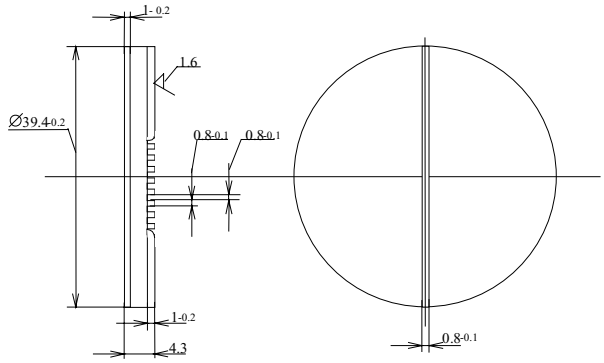

Figure 5. Heated substrate with channels for vapour removal. Dimensions and configuration can be modified

Some conclusions obtained up to now are:
- Metal fibre samples provide higher boiling heat transfer intensities, as compared to powder samples under similar conditions.
- For the metal fibrous samples the values of the heat transfer coefficient α reached values between 7 and 10·kW/m^2 K fort maximum heat flux density Q = 120 kW/m^2.
- At maximum heat flux densities Q = 30 to 60·kW/m^2, the powder samples heat transfer coefficients are 2 to times smaller than the corresponding values for the metal fibrous samples.
- Improvement of the contact of CS and awith a substrate (by sintering) samples resulted for the fibres in an increase of the heat transfer coefficients, as compared to pressing the samples to substrate. For the powder samples sintering leads to some decrease of the heat transfer intensity.
- Hybrid structures like "powder substrate plus fibre out layer" intensify the heat transfer process considerably, compared to powder samples

Figure 6 shows the heat transfer coefficient - heat flux density relation for two samples: Metal fibres and powder coated metal fibres.

The detailed analysis of all obtained data is out of the scope of this paper and will be discussed in future publications.

TESTS ON LHP WITH A FLAT "HEATING SURFACE TO POROUS STRUCTURE" INTERFACE

The from the previous work selected flat pore samples were incorporated in a LHP housing (diameter 44 mm, thickness 22 mm). The compensation chamber was arranged as a part of the housing and has an auxiliary wick Two tubes with diameter 3 mm provide the liquid/vapour transport to the condenser. The LHP test set-up is shown in figure 7. The temperature field was measured by the following thermocouples: T1, T2, T3 - Temperature of the heat input surface wall (unit 3 in figure 7); T4 - Temperature of the central part of the lid (unit 4); T5, T6, T7, T8, - Temperatures of the compensation chamber wall; T9 - Vapour temperature; T10 - Temperature of the liquid at the outlet of the condenser; T11 - Temperature of the coolant at the inlet of the condenser; T12 - Temperature of the coolant at the outlet from the condenser.

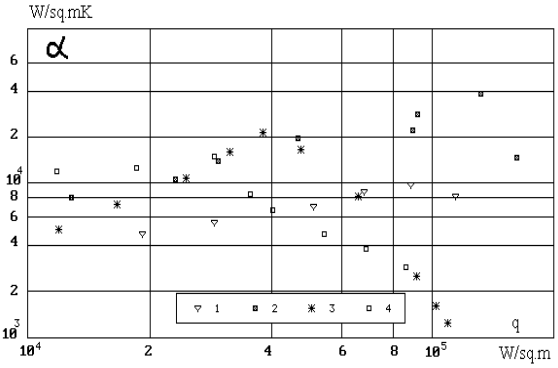

Figure 6. Comparison of the boiling curves of ethanol, for metal-fibrous and combined samples at constant pressure P = 0.3 bar:
1, 2 - fibre sample (66 % and d_{max} = 90 microns) pressed and sintered to the substrate respectively
3, 4 - hybrid sample pressed and sintered to substrate respectively.

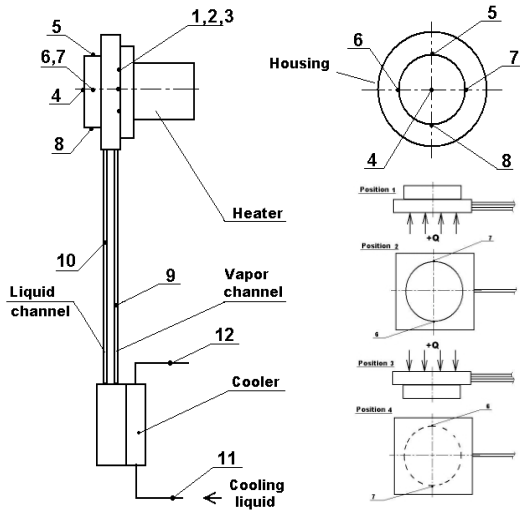

Figure 7. Schematic of LHP test set-up and orientation of the heat input with respect to gravity. Numbers are the thermocouples.

The thermal tests were conducted in loop heat pipes with flat evaporators. The characteristics of capillary pumps for these evaporators are

given in table 2. The following samples were used as capillary pumps:
- Metal felt samples of material X20H80, “Kyiv Polytechnic Institute”.
- Powder samples of Ni of Tais, Ltd (Moscow, Russia).
- Powder samples of Ti of the Ural State University (Ekaterinburg, Russia).

Table 2. The characteristics of capillary pumps for the flat evaporators of LHP test samples

No	Material	Diameter x width,	Porosity, %	Permeability, m^2	Maximum pore diameter,
1	X20 H80	39 x 3.7	35.9	$2.45 \cdot 10^{-13}$	12.0
2	Ni	39 x 7.9	66.0	$2.0 \cdot 10^{-14}$	2.4
3	Ti	39 x 7.3	57.0	$2.0 \cdot 10^{-13}$	10.4

Vapour removal grooves in the contact zone of the evaporator with a "hot" wall for LHP #1 and LHP#2 are made in a the wall of the evaporator body, and in LHP #3 directly in the plane of the capillary pump.

Figure 8 presents the experimentally determined heat transfer coefficient as a function of the transmitted heat flux density for LHP #1, for different values of the height of anti-gravity head *H*.

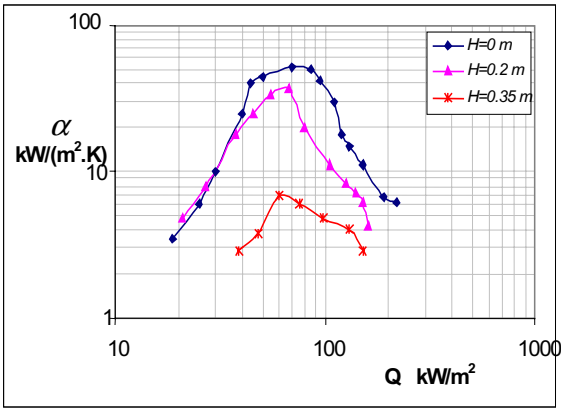

Figure 8. LHP #1: Heat transfer coefficient α versus power density Q for variable height.

It follows from this data that the function $\alpha(Q)$ has an extreme character. The value of heat transfer coefficient for the maximum heat flux is reduced with increasing height *H*. For LHP #1 the following maximum values of heat transfer coefficients α and heat flux densities Q are obtained:

-H = 0 m: α = 52·kW/m^2·K at Q = 70 kW/m^2.
-H = 0.2 m: α = 37·kW/m^2·K at Q = 67 kW/m^2.
- H = 0.35 m: α = 69 kW/m^2·K, Q = 60·kW/m^2.

It is necessary to note as well, that up to Q ≈ $4 \cdot 10^4$ W/m^2 the values α for a horizontal LHP orientation and for H = 0.2 m are close to each other. At the further rise of a thermal load the heat transfer intensity in horizontal orientation is higher. This can be explained by an earlier start of the heat-carrier replacement from larger pores on the evaporator surface. That results for LHP operation against gravity in an increase of a thermal resistance in the zone of the "hot" wall contact with the evaporator. This conclusion is confirmed by the much lower values of α (< 10 kW/m^2·K) obtained for H = 0.35 m. Obviously already during the LHP starting up in these conditions a lot of pores were drained in the contact zone of the evaporator and "hot" wall.

Figure 9 shows the outcomes for LHP #2, having a maximum pore diameter in the capillary pump evaporator being 5 times smaller than in LHP #1 (Table 2). The character of dependence $\alpha = f(Q)$ for LHP #2 is similar to the dependence obtained for LHP #1 (Fig. 8).

However, comparison of outcomes of these LHP’s shows that a decrease in maximum pore diameter of the evaporator considerably increases the potential to operate against a gravitational head.

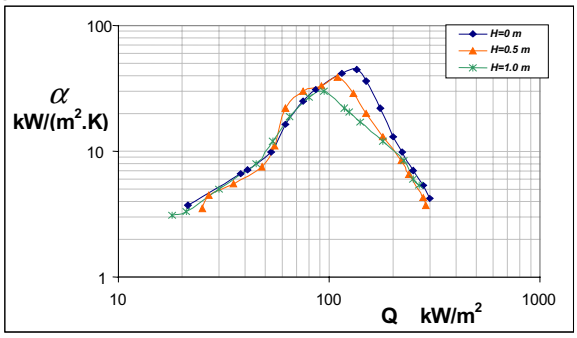

Figure 9. LHP #2: $\alpha = f(q)$ for variable *H*.

For LHP #2 the maximum values for heat transfer coefficients and heat flux densities are:
- H = 0 m: α = 45·kW/m^2·K, Q = 135·kW/m^2.
- H = 0.5 m: α = 39 kW/m^2·K,Q = 110·kW/m^2.
- H = 1 m: α = 30 kW/m^2·K, Q= 95·kW/m^2.

It follows from a comparison of data obtained for LHP #2 and for LHP #1 that, even for H = 0.35 m for LHP #1, the values of maximum heat flux densities and heat transfer coefficients are smaller than at H = 1 m for LHP #2. As one can

see in figure 9 for LHP #2, a zone of similarity of the maximum value of heat transfer coefficient relative to H essentially extends. The heat transfer intensity (up to $Q \approx 95 \cdot kW/m^2$) does not depend on the anti-gravity level, within the investigated range of H. The larger height adversely affects the operation of LHP #2 only after reaching the maximum heat transfer intensity for the given H. Here the maximum values of α are shifted to the area of larger heat flux densities in comparison with LHP #1.

The α versus Q curves, shown in the figures 8 and 9, have also an extreme character. At an increase of the heat flux density an increasing amount of new evaporation centres in the evaporator pores is initiated. It positively affects the heat transfer coefficients, as each new centre is an additional sink for heat from the heating zone. However, for an increase of Q the pressure, which is necessary to overcome by the capillary pump at transportation of a liquid to active evaporation centres, rises as well. It is clear that for an increase in temperature the menisci of the active centres deepen inside the evaporator, increasing the thermal resistance at the boundary "hot" wall - wick. Thus, for an increase of heat flux density two opposite effects will yield the net effect, determining the α-Q-relation.. The rise of heat transfer intensity in zone $Q < Q_{max}$ (Q_{max}- corresponds to maximum α) is explained by the prevailing influence of heat transfer intensification due to an increase of the amount of active evaporation centres. On the contrary, at $Q > Q_{max}$ the significant rise of thermal resistance due deepening of evaporating menisci inside the wick results in decrease in α.

As it follows from experimental data presented on figure 10, the character of $\alpha(Q)$ for LHP #3 essentially differs from similar curves obtained for LHP #1 and LHP #2. The main difference is the absence of pronounced maximum heat transfer intensity, and accordingly more mildly sloping character $\alpha(Q)$. Obviously, it is due to the fact that the vapour removal grooves in LHP #3 are directly inside the evaporator. The maximum α-values reached in LHP #3 are in 3 ÷ 5 times less, than corresponding values for LHP #1 and LHP #2 at the same H (exception - H= 0.35 m for LHP #1).

Figure 11 shows the power dependence of the temperature drop between heating zone vapour temperature and the temperature of the liquid exiting the condensation zone, for LHP #1.

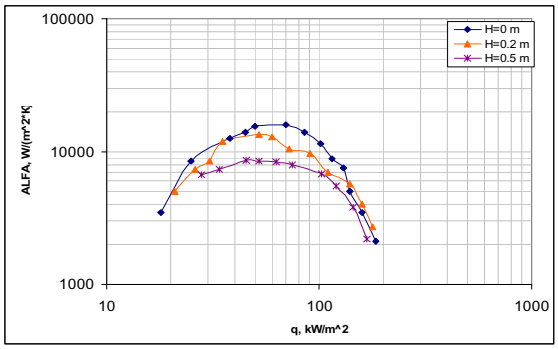

Figure 10. LHP #3: $\alpha = f(Q)$ for three H-values

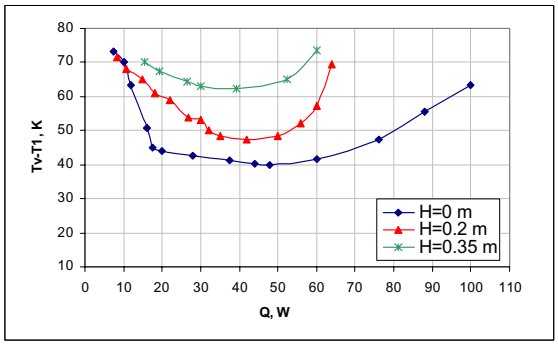

Figure 11. LHP #1: $(T_v - T_l) = f(Q)$ for three values of H

Obviously, at $Q > 10$ W the anti-gravity height essentially influences the temperature difference $T_v - T_l$. The power dependence of temperature difference has an extreme character, and the value of Q, corresponding to minimum drop $T_v - T_l$, is slightly reduced at increase in H.

The outcomes obtained in tests of LHP #2 (Fig. 12) show that height H in this case practically has no influence on drop $T_v - T_l$, in the investigated range of parameters.

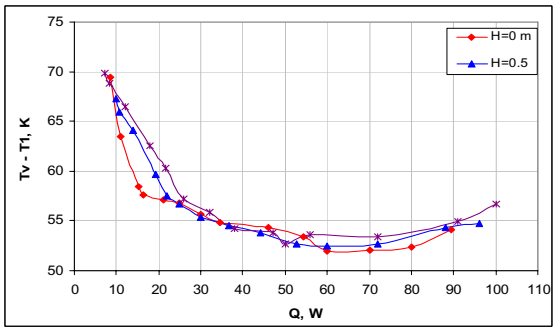

Figure 12. $(T_v - T_l) = f(Q)$ for LHP #2 for three values of H

The tests have shown that increase in H up to 0.2 m weakly influenced on T_v - T_l for LHP #3 (Fig. 13). However, at H = 0.5 m the temperature drop is already much more, than corresponding values at H = 0.2 m. The value of Q, for which T_v - T_l

reaches its minimum value for LHP #2, is in 1.5 to 2 times higher as compared with LHP #1 and LHP #3. This is due to the smaller pore size of the LHP #2 evaporator.

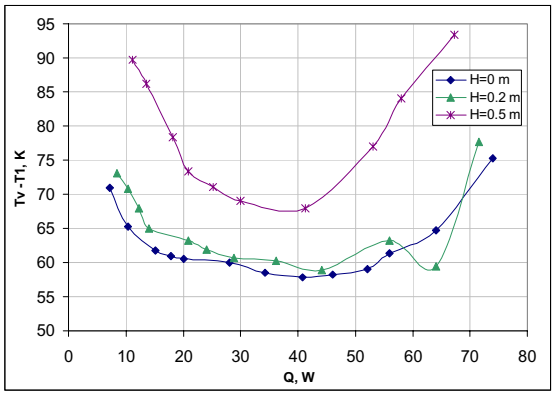

Figure 13. LHP #3: $(T_v - T_l) = f(Q)$ for three values of H

Figures 14 to 16 show the power dependence of the thermal resistance $R = (T_v - T_l) / Q$ for the three investigated loop heat pipes.

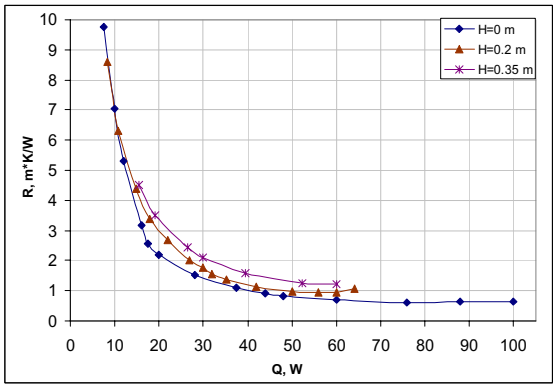

Figure 14. LHP #1: $R=f(Q)$ for three values of H

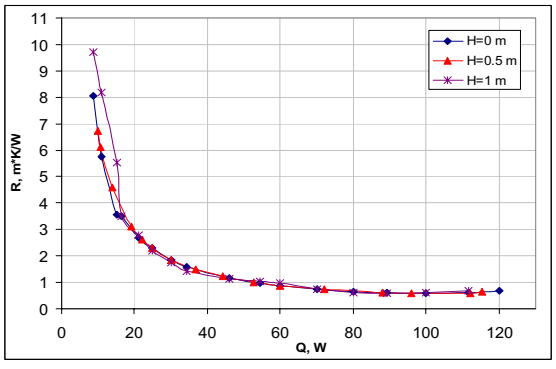

Figure 15. LHP #2: $R=f(Q)$ for three values of H

The values of R for all pipes are close to each other, at relatively low power (Q < 30 W). At large values of Q,, the thermal resistance of LHP #3 is slightly higher compared to LHP #1 and LHP #2. Figures for e.g. Q = 60 W are: LHP #1 1.22 K/W for H = 0.35 m; 0.96 K/W for LHP #2 at H = 1 m, 1.45 K/W for LHP #3 at H = 0.5 m. LHP #1 and LHP #3 show some increase in thermal resistance for increasing anti-gravity level. For LHP #2 this influence of H on the thermal resistance was not detected, within the investigated power range (Q = 10 to W). The thermal resistance of LHP #2, at H = 0.5 m, changes from 1.3 to 0.62 K/W, for Q ranging from 40 to 80 W. A value of 0.59 to 0.42 K/W was found elsewhere [2] for a LHP with a flat evaporator (under similar conditions, but with ammonia as the working fluid.

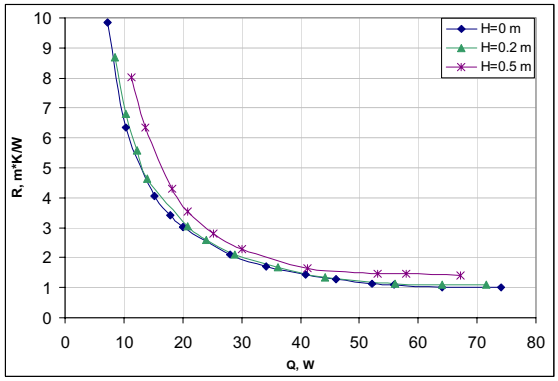

Figure 16. LHP #3: $R=f(Q)$ for three values of H

CONCLUSIONS

Tests with experimental models show that:

- Loop heat pipe characteristics depend on the porous evaporator parameters and on the way of vapour removal from the heating zone (locations of vapour removal channels).
- The heat transfer intensity, in the design with the layout of vapour removal grooves on the "hot" wall of the heat pipe evaporator body, is higher than for the layout with the grooves directly on the plane of the capillary pump.
- A decrease of a factor 5 of the maximum pore diameter in the capillary pump of the evaporator considerably increases heat flux densities when operating against gravity H (evaporator above condenser). For H = 1 m and the layout of grooves on the "hot" wall of the evaporator body LHP #2 reaches a heat transfer coefficient of α = 30 kW/(m^2·K) at maximum heat flux density Q = 95·kW/(m^2·K).
- A decrease of maximum pore diameter in the evaporator shifts the maximum of heat transfer intensity to larger thermal loads.
- An increase anti-gravity height (evaporator above condenser) results into an increase of the temperature drop between vapour in heating zone and liquid at the condenser

outlet, hence a LHP thermal resistance increase.

- In the investigated range of thermal loads (Q = 10 to 120 W), there is a strong influence of the anti-gravity height H on the thermal resistance of LHP #2, in which the capillary pump has a small pore size and vapour removal channels are on the evaporator "hot" wall.
- The thermal resistance of LHP #2, when removing the maximum heat fluxes operating against gravity, varies from 1.32 up to 0.62 K/W, for power values ranging from Q = 40 to 80 W.

References

1. Yu. Maidanik, S. Vershinin, M. Chernisheva, Development and Tests of Miniature Loop Heat Pipe with a Flat evaporator, Proc. 30th Int. Conference on Environmental Systems and the 7th European Symp. on Space Environmental Systems. July 10-13, 2000, Toulouse, France, Paper 2001-01-2491.
2. G. Gorbenko, P. Gakal, K. Maluhin, Mathematical model for steady state operation of loop heat pipe, Journal "Intergrovani Technologii Ta Energosberezhenniy" in Russian), 1999, N 4, pp. 60-68.